

Charm hadron physics at BESIII

Xiaokang Zhou^{*†}

University of Science and Technology of China, Hefei, China

E-mail: zhouxk@ustc.edu.cn

The BESIII Experiment at the Beijing Electron Positron Collider (BEPCII) has accumulated the world's largest e^+e^- collision samples at $\psi(3770)$ peak, at 4.178 GeV for $D_S^{*+}D_S^-$ decay and at the $\Lambda_c^+\bar{\Lambda}_c^-$ pair mass threshold, which allow us to study decays of charmed mesons and baryons in a uniquely clean background. In this report, recent results in charm hadronic decay at BESIII will be presented.

The 15th International Conference on Flavor Physics & CP Violation

5-9 June 2017

Prague, Czech Republic

^{*}Speaker.

[†]on behalf of the BESIII collaboration.

1. Introduction

The analyses presented in this report are based on two data samples collected by the BESIII detector[1], installed at the double-ring BEPCII collider (IHEP, Beijing, P.R.C). One is the largest e^+e^- annihilation sample in the world to date, $2.92 fb^{-1}$, at the 3.773 GeV center-of-mass energy, where $e^+e^- \rightarrow \psi(3770) \rightarrow D\bar{D}$ is mainly produced. Another one is the unique and largest, $0.5 fb^{-1}$, at the center-of-mass energy of 4.599 GeV which is the $\Lambda_c^+ \bar{\Lambda}_c^-$ mass threshold.

We make use of double-tag technique initially used by MARK III [2] to identify the $D\bar{D}/\Lambda_c^+ \bar{\Lambda}_c^-$. In this technique, the yields of single tags (ST), where one D/Λ_c is reconstructed in the tag modes, and double tags (DT), where both D/Λ_c mesons are reconstructed, are determined. In this report, \bar{D}^0 is reconstructed in one of three tag modes: $\bar{D}^0 \rightarrow K^+ \pi^-$, $K^+ \pi^- \pi^0$ and $K^+ \pi^- \pi^+ \pi^-$, while D^- is reconstructed in one of six tag modes: $D^- \rightarrow K^+ \pi^- \pi^-$, $K^+ \pi^- \pi^- \pi^0$, $K_S^0 \pi^-$, $K_S^0 \pi^- \pi^0$, $K_S^0 \pi^- \pi^- \pi^+$ and $K^+ K^- \pi^-$, while Λ_c^+ is reconstructed in one of twelve tag modes: $\Lambda_c^+ \rightarrow p K_S^0$, $p K^- \pi^+$, $p K_S^0 \pi^0$, $p K_S^0 \pi^+ \pi^-$, $p K^- \pi^+ \pi^0$, $\Lambda \pi^+$, $\Lambda \pi^+ \pi^0$, $\Lambda \pi^+ \pi^- \pi^+$, $\Sigma^0 \pi^+$, $\Sigma^+ \pi^0$, $\Sigma^+ \pi^+ \pi^-$ and $\Sigma^+ \omega$. The hadronic decays are identified using the beam-constrained mass $M_{BC} = \sqrt{E_{\text{beam}}^2 - p^2 c^2}$, where E_{beam} is the beam energy and p is measured momentum of $D^-/\bar{D}^0/\Lambda_c^+$ and energy difference $\Delta E = E_{\text{beam}} - E$, where E is the measured energy of $D^-/\bar{D}^0/\Lambda_c^+$. Throughout this report, the inclusion of charge conjugated processes is implied, unless otherwise explicitly mentioned.

In this proceeding, four measurements of D hadronic decays and four measurements of Λ_c hadronic decays are reported.

2. D hadronic decays

2.1 Absolute branching fraction (BF) of $D^0 \rightarrow K_S^0/K_L^0 \pi^0(\pi^0)$ and y_{CP} measurement (preliminary)

Non-leptonic D decays and their strong phases have been of great interest as they are essentially related to the studies of CP violation (CPV), $D\bar{D}$ mixing and SU(3) symmetry breaking effects in charm physics. As first pointed out by I.I.Bigi and H.Yamamoto [3], the decay rates of $D \rightarrow K_S^0 \pi$ and $D \rightarrow K_L^0 \pi$ are not the same because of the interference of the Cabibbo-favored (CF) component $D \rightarrow K^0 \pi$ with the doubly Cabibbo-suppressed (DCS) component $D \rightarrow \bar{K}^0 \pi$. Since the interference of K^0 with \bar{K}^0 is opposite for K_S^0 and K_L^0 , $\mathcal{B}_{D \rightarrow K_S^0 \pi^0}$ and $\mathcal{B}_{D \rightarrow K_L^0 \pi^0}$ should not in general be equal. The scale of the asymmetry is set by the DCS factor $\tan^2 \theta_C \approx 0.05$, where θ_C is the Cabibbo angle.

In BF measurement of $D^0 \rightarrow K_S^0/K_L^0 \pi^0(\pi^0)$, the quantum correlation should be considered [4]. In the absence of CPV and $D\bar{D}$ mixing, the CP eigenstate BF is extracted by $\mathcal{B}_{CP\pm} = \frac{1}{1 \mp C_f} \frac{N_{CF,CP\pm}/\varepsilon}{N_{CF}}$, ($C_f \equiv \frac{2r \cos \delta}{1+r^2}$), where $N_{CF,CP\pm}$ (N_{CF}) denote the DT (ST) yields, ε is the signal efficiency, C_f is a correction factor derived from r and δ , r is the ratio of the DCS to CF amplitudes for $D^0(\bar{D}^0)$ decays to the same CF final state, and δ is the strong phase difference between the two amplitudes. C_f can be measured using the $CP\pm$ ST events and CF vs. $CP\pm$ DT events. The asymmetries of the BFs of $D^0 \rightarrow K_S^0/K_L^0 \pi^0(\pi^0)$ can be determined by $R(D^0 \rightarrow K_S^0/K_L^0 \pi^0(\pi^0)) = \frac{\mathcal{B}_{K_S^0 \pi^0(\pi^0)} - \mathcal{B}_{K_L^0 \pi^0(\pi^0)}}{\mathcal{B}_{K_S^0 \pi^0(\pi^0)} + \mathcal{B}_{K_L^0 \pi^0(\pi^0)}}$. The results can be found in Table 1, which agree well with the measurement of CLEO-c[5].

Table 1: BFs and asymmetries of $D^0 \rightarrow K_S^0/K_L^0\pi^0(\pi^0)$. The uncertainties in each tag are statistical only. The first uncertainties in average results are statistical and the second are systematic.

tag modes	$\mathcal{B}_{K_S^0\pi^0}(\%)$	$\mathcal{B}_{K_L^0\pi^0}(\%)$	$R(D^0 \rightarrow K_S^0/K_L^0\pi^0)$
$K\pi$	1.218 ± 0.042	1.062 ± 0.038	0.069 ± 0.025
$K\pi\pi\pi$	1.225 ± 0.037	0.987 ± 0.036	0.107 ± 0.023
$K\pi\pi^0$	1.254 ± 0.029	0.959 ± 0.028	0.133 ± 0.018
Average	$1.237 \pm 0.020 \pm 0.033$	$0.993 \pm 0.019 \pm 0.029$	$0.109 \pm 0.012 \pm 0.018$
tag modes	$\mathcal{B}_{K_S^0\pi^0\pi^0}(\%)$	$\mathcal{B}_{K_L^0\pi^0\pi^0}(\%)$	$R(D^0 \rightarrow K_S^0/K_L^0\pi^0\pi^0)$
$K\pi$	1.025 ± 0.049	1.299 ± 0.081	-0.118 ± 0.039
$K\pi\pi\pi$	0.935 ± 0.043	1.298 ± 0.076	-0.162 ± 0.036
$K\pi\pi^0$	1.065 ± 0.036	1.259 ± 0.060	-0.084 ± 0.029
Average	$1.015 \pm 0.024 \pm 0.042$	$1.280 \pm 0.041 \pm 0.062$	$-0.116 \pm 0.020 \pm 0.028$

Oscillations between meson and anti-meson, also called mixing, can occur when the flavor eigenstates differ from the physical mass eigenstates. These effects provide a mechanism whereby interference in the transition amplitudes of mesons and anti-mesons may occur. The oscillations are conventionally characterized by two dimensionless parameters $x = \Delta m/\Gamma$ and $y = \Delta\Gamma/\Gamma$. In the absence of CP violation, one has $y_{CP} = y$.

We partly reconstruct the D or \bar{D} which decays to $Ke\nu$ and fully reconstruct the other \bar{D} or D which decays to K_S^0/K_L^0 . When considering $D\bar{D}$ mixing without CPV, y_{CP} then can be determined by $y_{CP} = \frac{L_{K_S^0} - L_{K_L^0}}{L_{K_S^0} + L_{K_L^0}}$, where $L_{K_S^0/K_L^0} = \frac{N_{K_S^0/K_L^0\pi^0,Ke\nu}/\varepsilon_{K_S^0/K_L^0\pi^0,Ke\nu}}{N_{K_S^0/K_L^0\pi^0}/\varepsilon_{K_S^0/K_L^0\pi^0}}$, $N_{K_S^0/K_L^0\pi^0,Ke\nu}$ ($N_{K_S^0/K_L^0\pi^0}$) are the DT(ST) yields, $\varepsilon_{K_S^0/K_L^0\pi^0,Ke\nu}$ ($\varepsilon_{K_S^0/K_L^0\pi^0}$) are the DT(ST) efficiencies. We obtain $y_{CP} = (1.6 \pm 2.5_{stat.})\%$, which is consistent with previous BESIII measurement with more tag modes [6].

2.2 Absolute BF measurement of $D^+ \rightarrow K_S^0/K_L^0K^+(\pi^0)$ (preliminary)

Experimental studies of the hadronic decays of charm mesons can shed light on the interplay between the strong and weak forces. In the standard model (SM), the singly Cabibbo-suppressed (SCS) D meson hadronic decays are predicted to exhibit CP asymmetries of the order of 10^{-3} [7]. Direct CP violation in SCS decays could arise from the interference between tree-level and penguin decay processes. Consequently, any observation of CP asymmetry greater than $\mathcal{O}(10^{-3})$ in any SCS D hadronic decay would be evidence for new physics beyond the SM [8]. This talk reports the measurements of the absolute BFs and the CP asymmetries of the SCS decays of $D^+ \rightarrow K_S^0K^+, K_S^0K^+\pi^0, K_L^0K^+$ and $K_L^0K^+\pi^0$. Note that the decay rates of $D^+ \rightarrow K_S^0K^+(\pi^0)$ and $D^+ \rightarrow K_L^0K^+(\pi^0)$ are the same because there is no interference of $K^0 - \bar{K}^0$. The measurement of the BF of the two body decay $D^+ \rightarrow K_S^0K^+$ is also helpful for better understanding SU(3)-violating effects in D meson decays [9].

According to the DT method, the absolute BF for the signal decay is described by $\mathcal{B}_{sig} = \frac{N_{DT}/\varepsilon_{DT}}{N_{ST}/\varepsilon_{ST}}$, where N_{DT} (N_{ST}) and ε_{DT} (ε_{ST}) are the yields and efficiencies of DT(ST) modes. With the measured absolute BFs of D^+ and D^- decays (\mathcal{B}_{sig}^+ and \mathcal{B}_{sig}^-), the CP asymmetry for the decay of interest can be determined by $A_{CP} = \frac{\mathcal{B}_{sig}^+ - \mathcal{B}_{sig}^-}{\mathcal{B}_{sig}^+ + \mathcal{B}_{sig}^-}$. The results are shown in Table. 2. The BF of K_S^0K

Table 2: Summary of the measured BFs and CP asymmetries, where the first and second uncertainties are statistical and systematic, respectively, and a comparison with the world average value [10]

signal mode	$\mathcal{B}_{D^+}(\times 10^{-3})$	$\mathcal{B}_{D^-}(\times 10^{-3})$	$\bar{\mathcal{B}}(\times 10^{-3})$	$\mathcal{B}_{PDG}(\times 10^{-3})$	$A_{CP}(\%)$
$K_S^0 K^\pm$	$3.01 \pm 0.12 \pm 0.08$	$3.10 \pm 0.12 \pm 0.08$	$3.06 \pm 0.09 \pm 0.08$	2.95 ± 0.15	$-1.5 \pm 2.8 \pm 1.6$
$K_S^0 K^\pm \pi^0$	$5.23 \pm 0.28 \pm 0.24$	$5.09 \pm 0.29 \pm 0.22$	$5.16 \pm 0.21 \pm 0.23$	-	$1.4 \pm 4.0 \pm 2.4$
$K_L^0 K^\pm$	$3.13 \pm 0.14 \pm 0.10$	$3.32 \pm 0.15 \pm 0.11$	$3.23 \pm 0.11 \pm 0.11$	-	$-3.0 \pm 3.2 \pm 1.2$
$K_L^0 K^\pm \pi^0$	$5.17 \pm 0.30 \pm 0.21$	$5.26 \pm 0.30 \pm 0.21$	$5.22 \pm 0.22 \pm 0.21$	-	$-0.9 \pm 4.1 \pm 1.6$

is consistent with CLEO-c's measurement [11], the BFs of $K_S^0 K \pi^0$, $K_L^0 K$ and $K_L^0 K \pi^0$ are measured for the first time. No evidence of CP asymmetries are found for the 4 SCS decays.

2.3 BF measurement of some $D^{0(+)} \rightarrow PP$ (preliminary)

The two-body hadronic decays $D \rightarrow P_1 P_2$ (P denotes one of pseudoscalar mesons) serve as an ideal testbed to improve the understanding of the weak and strong interactions in decays of charmed mesons. Due to the relatively simple topology, the amplitude of each $D \rightarrow P_1 P_2$ decay can be theoretically derived as a sum of different diagrams based on SU(3)-flavor symmetry [12]. Comprehensive and improved experimental measurements of the BFs for these decays will help to validate the theoretical calculations. Moreover, these measurements will provide important and complementary data to explore SU(3)-flavor symmetry breaking effects in hadronic decays of the D mesons [13, 14, 15, 16].

Table 3: Measured BFs of $D^{+(0)} \rightarrow P_1 P_2$ ($\mathcal{B}_{thiswork}$), the first and second uncertainties are statistical and systematic, respectively. The world average values (\mathcal{B}_{PDG}) are also shown.

mode	$\mathcal{B}_{thiswork}(\times 10^{-3})$	$\mathcal{B}_{PDG}(\times 10^{-3})$	mode	$\mathcal{B}_{thiswork}(\times 10^{-3})$	$\mathcal{B}_{PDG}(\times 10^{-3})$
$D^+ \rightarrow \pi^+ \pi^0$	$1.259 \pm 0.033 \pm 0.025$	1.24 ± 0.06	$D^0 \rightarrow \pi^+ \pi^-$	$1.508 \pm 0.018 \pm 0.027$	1.421 ± 0.025
$D^+ \rightarrow K^+ \pi^0$	$0.231 \pm 0.021 \pm 0.006$	0.189 ± 0.025	$D^0 \rightarrow K^+ K^-$	$4.233 \pm 0.021 \pm 0.076$	4.01 ± 0.07
$D^+ \rightarrow \pi^+ \eta$	$3.790 \pm 0.070 \pm 0.076$	3.66 ± 0.22	$D^0 \rightarrow K^\mp \pi^\pm$	$38.98 \pm 0.06 \pm 0.62$	39.4 ± 0.4
$D^+ \rightarrow K^+ \eta$	$0.151 \pm 0.025 \pm 0.014$	0.112 ± 0.018	$D^0 \rightarrow K_S^0 \pi^0$	$12.39 \pm 0.06 \pm 0.30$	12.0 ± 0.4
$D^+ \rightarrow \pi^+ \eta'$	$5.12 \pm 0.14 \pm 0.21$	4.84 ± 0.31	$D^0 \rightarrow K_S^0 \eta$	$5.13 \pm 0.07 \pm 0.12$	4.85 ± 0.30
$D^+ \rightarrow K^+ \eta'$	$0.164 \pm 0.051 \pm 0.025$	0.183 ± 0.023	$D^0 \rightarrow K_S^0 \eta'$	$9.49 \pm 0.20 \pm 0.37$	9.5 ± 0.5
$D^+ \rightarrow K_S^0 \pi^+$	$15.91 \pm 0.06 \pm 0.33$	15.3 ± 0.6			
$D^+ \rightarrow K_S^0 K^+$	$3.183 \pm 0.029 \pm 0.067$	2.95 ± 0.15			

ST method is used in this analysis and the BF of the $D^{+(0)} \rightarrow P_1 P_2$ decay is determined by $\mathcal{B}_{D^{+(0)} \rightarrow P_1 P_2} = \frac{N_{net}}{2 \cdot N_{D^+ D^- (D^0 \bar{D}^0)}^{tot} \cdot \epsilon(\cdot \mathcal{B}_i)}$, where N_{net} is the background-subtracted signal yields observed in data, $N_{D^+ D^- (D^0 \bar{D}^0)}^{tot}$ is the total number of $D^+ D^- (D^0 \bar{D}^0)$ pairs, ϵ is the detection efficiency obtained by the MC simulation, and \mathcal{B}_i denotes the BFs of the intermediate resonances π^0, η, K_S^0 and η' . Results are shown in Table 3. Our results are consistent with the world average values within uncertainties and the BFs of $D^+ \rightarrow \pi^+ \pi^0, \pi^+ \eta, \pi^+ \eta', K_S^0 \pi^+, K_S^0 K^+$ and $D^0 \rightarrow K_S^0 \pi^0, K_S^0 \eta, K_S^0 \eta'$ are determined with improved precision. The measured BFs for $D^0 \rightarrow K_S^0 \pi^0$ and $D^+ \rightarrow K_S^0 K^+$ are

consistent with those measured using DT technique in Sec. 2.1 and 2.2, but with better precision. These results will be useful for tests of theoretical calculations and to provide a better understanding of SU(3)-flavor symmetry breaking effects in hadronic decays of the $D^{+(0)}$ mesons.

2.4 BF measurement of $D^{0(+)} \rightarrow 2K_S^0 + X$

In this report, we measure the BFs for the hadronic decays $D^+ \rightarrow K_S^0 K_S^0 \pi^+$, $D^0 \rightarrow K_S^0 K_S^0$, $D^+ \rightarrow K_S^0 K_S^0 K^+$ and $D^0 \rightarrow K_S^0 K_S^0 K_S^0$. These decays have simpler event topologies and suffer less from combinatorial backgrounds than other decay modes containing two K_S^0 in the final state. The comprehensive or improved measurements of three-body decays will benefit the understanding of the interplay between the weak and strong interactions in multi-body decays where theoretical predictions are poorer than two-body decays. The improved measurements of two-body decays can serve to better explore the contributions of W-exchange diagrams and final-state interactions [17, 18, 19, 20], as well as SU(3)-flavor symmetry breaking effects [21, 22, 14, 23, 24] in D meson decays. In addition, these measurements will also help to improve background estimations in the precision measurements of D and B meson decays.

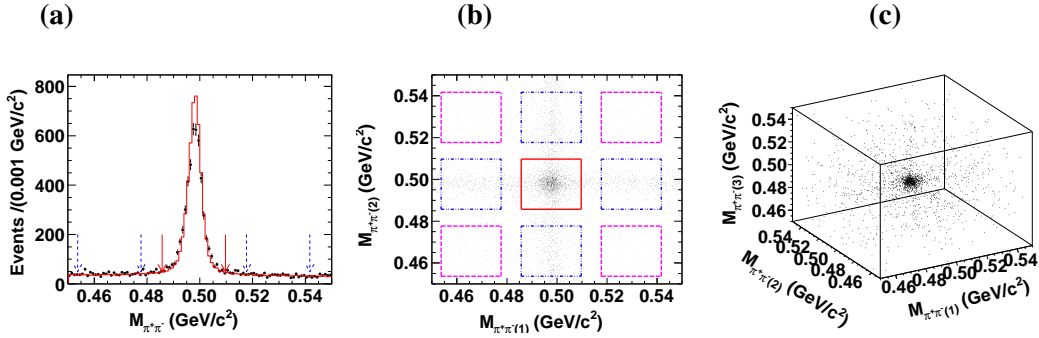


Figure 1: (a) Comparison of the $M_{\pi^+\pi^-}$ distributions of the $D^0 \rightarrow K_S^0 K_S^0$ candidate events between data (dots with error bars) and inclusive MC (histogram). The pairs of the solid (dashed) arrows denote the K_S^0 signal (sideband) regions. (b) Distribution of $M_{\pi^+\pi^-(1)}$ versus $M_{\pi^+\pi^-(2)}$ for the $D^0 \rightarrow K_S^0 K_S^0$ candidate events in data. (c) Distribution of $M_{\pi^+\pi^-(1)}$ versus $M_{\pi^+\pi^-(2)}$ versus $M_{\pi^+\pi^-(3)}$ for the $D^0 \rightarrow K_S^0 K_S^0 K_S^0$ candidate events in data.

ST method is used in this analysis. The main peaking background come from similar-final-states D decay but $\pi^+\pi^-$ pairs do not form K_S^0 . Thus, two-dimensional (2D) signal and sideband regions are defined. Figure 1(b) shows the distribution of $M_{\pi^+\pi^-(1)}$ versus $M_{\pi^+\pi^-(2)}$ for the $D^0 \rightarrow K_S^0 K_S^0$ candidate events in data. The solid box, in which both of the $\pi^+\pi^-$ combinations lie in the K_S^0 signal regions, denotes the 2D signal region. The dot-dashed (dashed) boxes indicate the 2D sideband 1 (2) regions, in which one (two) of the $\pi^+\pi^-$ combinations lie in the K_S^0 sideband regions and the others are in the K_S^0 signal region. For the $D^0 \rightarrow K_S^0 K_S^0 K_S^0$ decay, $M_{\pi^+\pi^-(1)}$ versus $M_{\pi^+\pi^-(2)}$ versus $M_{\pi^+\pi^-(3)}$ of the candidate events in data is shown in Fig. 1 (c). The region in which all three $\pi^+\pi^-$ combinations lie in the K_S^0 signal regions is taken as the three-dimensional (3D) signal region. The 3D sideband i ($i = 1, 2, 3$) regions denote those in which i of the three $\pi^+\pi^-$ pairs lie in the K_S^0 sideband regions and the rest are located in the K_S^0 signal regions.

The net numbers of the $D^0 \rightarrow K_S^0 K_S^0$, $D^+ \rightarrow K_S^0 K_S^0 K^+$ can be calculated by $N_{\text{net}} = N_{K_S^0 \text{sig}} - \frac{1}{2}N_{\text{sb1}} + \frac{1}{4}N_{\text{sb2}} - N_{\text{other}}^b$, while $D^0 \rightarrow K_S^0 K_S^0 K_S^0$ can be calculated by $N_{\text{net}} = N_{K_S^0 \text{sig}} - \frac{1}{2}N_{\text{sb1}} + \frac{1}{4}N_{\text{sb2}} -$

$\frac{1}{4}N_{\text{sb3}} - N_{\text{other}}^b$. Then the BF is determined by $\mathcal{B}_{D^{+(0)} \rightarrow f} = \frac{N_{\text{net}}}{2 \cdot \sigma_{D^+D^-} \cdot \mathcal{L} \cdot \varepsilon}$, where ε is the detection efficiency including the BF of $K_S^0 \rightarrow \pi^+\pi^-$, \mathcal{L} is the integrated luminosity of data [25] and $\sigma_{D^+D^-}$ ($D^0\bar{D}^0$) is the D^+D^- ($D^0\bar{D}^0$) cross section at the $\psi(3770)$ resonance peak [26]. Finally, we obtain these BFs in Table 4, compare to PDG value [10], BF of $D^+ \rightarrow K_S^0 K_S^0 \pi^+$ is measured for the first time and others are consistent with previous measurements, but with much improved precision. For more details about this analysis refer to [27].

Table 4: Comparisons of the BFs (in 10^{-4}) measured in this work with the PDG values [10].

Decay modes	This work	PDG
$D^+ \rightarrow K_S^0 K_S^0 K^+$	$25.4 \pm 0.5 \pm 1.2$	45 ± 20
$D^+ \rightarrow K_S^0 K_S^0 \pi^+$	$27.0 \pm 0.5 \pm 1.2$	-
$D^0 \rightarrow K_S^0 K_S^0$	$1.67 \pm 0.11 \pm 0.11$	1.7 ± 0.4
$D^0 \rightarrow K_S^0 K_S^0 K_S^0$	$7.21 \pm 0.33 \pm 0.44$	9.1 ± 1.3

3. Λ_c^+ hadronic decays

3.1 BR measurement of $\Lambda_c^+ \rightarrow \Sigma^- \pi^+ \pi^+$ and $\Lambda_c^+ \rightarrow \Sigma^- \pi^+ \pi^+ \pi^0$

More than 30 years have passed since the Λ_c^+ baryon was first observed in e^+e^- annihilations by the Mark II experiment [28] and the knowledge of Λ_c^+ decays remains very poor compared to that for charmed mesons. So far, measured decay modes account for only about 60% [10] of all Λ_c^+ decays, primarily consisting of modes with a $\Lambda(\Sigma)$ hyperon or a proton in the final state. Decays to the Σ^- hyperon are Cabibbo-allowed and are expected to have large rates. However, no experimental measurements exist except for $\Lambda_c^+ \rightarrow \Sigma^- \pi^+ \pi^+$ [10]. Therefore, searching for additional decay modes with Σ^- in the final state is important to build up knowledge on Λ_c^+ decays.

DT method is used and the Σ^- hyperon is detected through $\Sigma^- \rightarrow n\pi^-$. As the neutron is not reconstructed in this analysis, we deduce its kinematic properties by four-momentum conservation. The distributions of M_n versus $M_{n\pi^-}$ for the $\Lambda_c^+ \rightarrow \Sigma^- \pi^+ \pi^+$ and $\Lambda_c^+ \rightarrow \Sigma^- \pi^+ \pi^+ \pi^0$ candidates in data are shown in Figs. 2 (a) and (b), respectively, where clusters corresponding to signal decays are evident. To improve the resolution of the signal mass, as well as to better handle the backgrounds around the Σ^- and neutron mass regions, we determine the signal yields from the distribution of the mass difference $M_{n\pi^-} - M_n$, since $M_{n\pi^-}$ and M_n are highly correlated. Based on a study of the inclusive MC samples, no peaking backgrounds are expected for these two channels.

The absolute BFs for $\Lambda_c^+ \rightarrow \Sigma^- \pi^+ \pi^+$ and $\Lambda_c^+ \rightarrow \Sigma^- \pi^+ \pi^+ \pi^0$ are determined by $\mathcal{B}_{\Lambda_c^+ \rightarrow \Sigma^- \pi^+ \pi^+ (\pi^0)} = \frac{N_{\Sigma^- \pi^+ \pi^+ (\pi^0)}^{\text{obs}}}{N_{\Lambda_c^+}^{\text{tot}} \cdot \varepsilon_{\Sigma^- \pi^+ \pi^+ (\pi^0)} \cdot \mathcal{B}_{\Sigma^- \rightarrow n\pi^-}}$, where $\varepsilon_{\Sigma^- \pi^+ \pi^+ (\pi^0)}$ is the detection efficiency for the $\Lambda_c^+ \rightarrow \Sigma^- \pi^+ \pi^+ (\pi^0)$ decay with $\Sigma^- \rightarrow n\pi^-$. The intermediate decay BF of $\Sigma^- \rightarrow n\pi^-$ is included in the denominator. We obtain $\mathcal{B}_{\Lambda_c^+ \rightarrow \Sigma^- \pi^+ \pi^+} = (1.81 \pm 0.17 \pm 0.09)\%$ and $\mathcal{B}_{\Lambda_c^+ \rightarrow \Sigma^- \pi^+ \pi^+ \pi^0} = (2.11 \pm 0.33 \pm 0.14)\%$, where the first uncertainties are statistical, and the second are systematic, respectively. This is the first observation of the decay $\Lambda_c^+ \rightarrow \Sigma^- \pi^+ \pi^+ \pi^0$ and the first absolute BF measurement for $\Lambda_c^+ \rightarrow \Sigma^- \pi^+ \pi^+$. Our result for $\mathcal{B}_{\Lambda_c^+ \rightarrow \Sigma^- \pi^+ \pi^+}$ is consistent with and more precise than the previous result [10]. For more details about this analysis refer to [29].

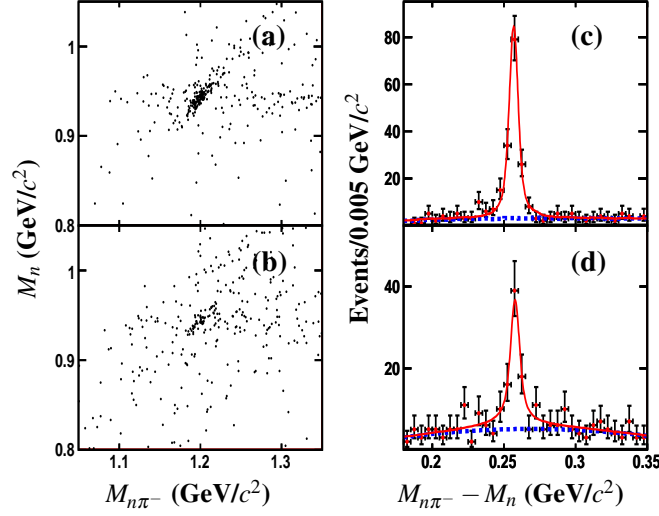


Figure 2: Scatter plots of M_n versus $M_{n\pi^-}$ for candidates in data for (a) $\Lambda_c^+ \rightarrow \Sigma^- \pi^+ \pi^+$ and (b) $\Lambda_c^+ \rightarrow \Sigma^- \pi^+ \pi^+ \pi^0$. Also shown are fits to the distributions of $M_{n\pi^-} - M_n$ for (c) $\Lambda_c^+ \rightarrow \Sigma^- \pi^+ \pi^+$ and (d) $\Lambda_c^+ \rightarrow \Sigma^- \pi^+ \pi^+ \pi^0$ in data. Solid lines are the results of a complete fit while dashed lines reflect the background components.

3.2 $\Lambda_c^+ \rightarrow p\pi^+\pi^-$ and $\Lambda_c^+ \rightarrow pK^+K^-$

In contrast to the charmed meson decays, which are usually dominated by factorizable amplitudes, decays of charmed baryons receive sizable nonfactorizable contributions from W -exchange diagrams, which are subject to color and helicity suppression. The study of nonfactorizable contributions is critical to understand the dynamics of charmed baryon decays. The SCS decay $\Lambda_c^+ \rightarrow p\pi^+\pi^-$ proceeds via the external W -emission, internal W -emission and W -exchange processes, while the SCS decay $\Lambda_c^+ \rightarrow pK^+K^-$ proceeds via the internal W -emission and W -exchange diagrams only. Precisely measuring and comparing their BFs may help to reveal the Λ_c internal dynamics [30]. A measurement of the SCS mode $\Lambda_c^+ \rightarrow p\phi$ is of particular interest because it receives contributions only from the internal W -emission diagrams, which can reliably be obtained by a factorization approach [30]. An improved measurement of the $\Lambda_c^+ \rightarrow p\phi$ BF is thus essential to validate theoretical models and test the application of large- N_c factorization in the charmed baryon sector [31], where, N_c is the number of colors.

Table 5: Summary of relative and absolute BFs, and comparing with the results from PDG [10]. Uncertainties are statistical, experimental systematic, and reference mode uncertainty, respectively.

Decay modes	$\mathcal{B}_{\text{mode}}$ (This work)	$\mathcal{B}_{\text{mode}}$ (PDG average)
$\Lambda_c^+ \rightarrow p\pi^+\pi^-$	$(3.91 \pm 0.28 \pm 0.15 \pm 0.24) \times 10^{-3}$	$(3.5 \pm 2.0) \times 10^{-3}$
$\Lambda_c^+ \rightarrow p\phi$	$(1.06 \pm 0.19 \pm 0.08 \pm 0.06) \times 10^{-3}$	$(8.2 \pm 2.7) \times 10^{-4}$
$\Lambda_c^+ \rightarrow pK^+K^-$ (non- ϕ)	$(5.47 \pm 1.30 \pm 0.41 \pm 0.33) \times 10^{-4}$	$(3.5 \pm 1.7) \times 10^{-4}$

ST method is used and $\Lambda_c^+ \rightarrow pK^- \pi^+$ is reconstructed as the reference mode. Fig 3 shows the fit results. In the decay $\Lambda_c^+ \rightarrow p\pi^+\pi^-$, the peaking background come from the decays $\Lambda_c^+ \rightarrow \Lambda\pi^+$

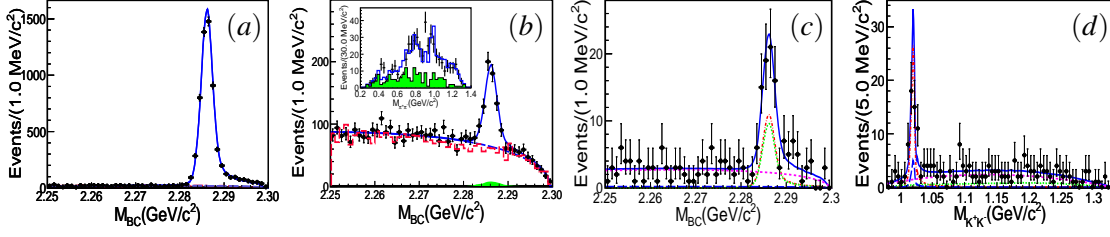


Figure 3: Distributions of M_{BC} for the decays (a) $\Lambda_c^+ \rightarrow pK^-\pi^+$, (b) $\Lambda_c^+ \rightarrow p\pi^+\pi^-$, (c) $\Lambda_c^+ \rightarrow pK^+K^-$ and (d) $M_{K^+K^-}$ for $\Lambda_c^+ \rightarrow pK^+K^-$. Points with an error bar are data, the blue solid lines show the total fits, the blue long dashed lines are the combinatorial background shapes, and the red long dashed histograms are data from the ΔE sideband region for comparison. In (b), the green shaded histogram is the peaking background from the CF decays $\Lambda_c^+ \rightarrow pK_S^0$ and $\Lambda_c^+ \rightarrow \Lambda\pi$. The inset plot in (b) shows the $\pi^+\pi^-$ invariant mass distribution with the additional requirement $|\Delta E| < 8$ MeV and $2.2836 < M_{BC} < 2.2894$ GeV/c², where the dots with an error bar are for the data, the blue solid histogram shows the fit curve from PWA, and the green shaded histogram shows background estimated from the M_{BC} sideband region. In (c) and (d), the blue solid curves are for the total fit results, the red dash-dotted curves show the $\Lambda_c^+ \rightarrow p\phi \rightarrow pK^+K^-$ signal, the green dotted curves show the $\Lambda_c^+ \rightarrow pK^+K_{non-\phi}^-$ signal, the blue long-dashed curves are the background with ϕ production, and the magenta dashed curves are the non- ϕ background.

and $\Lambda_c^+ \rightarrow pK_S^0$. For the decay $\Lambda_c^+ \rightarrow pK^+K^-$, we perform a two-dimensional unbinned extended maximum likelihood fit to estimate the ϕ and non- ϕ process. The results are shown in Table. 5, we present the first observation of the SCS decays $\Lambda_c^+ \rightarrow p\pi^+\pi^-$ and improved (or comparable) measurements of the $\Lambda_c^+ \rightarrow p\phi$ and $\Lambda_c^+ \rightarrow pK^+K_{non-\phi}^-$ BFs comparing to PDG values [10]. The relative BFs with respect to the CF decay $\Lambda_c^+ \rightarrow pK^-\pi^+$ are measured. The results provide important data to understand the dynamics of Λ_c^+ decays. They especially help to distinguish predictions from different theoretical models and understand contributions from factorizable effects [30]. More details can be found in Ref. [33].

3.3 $\Lambda_c^+ \rightarrow p^+\eta$ and $\Lambda_c^+ \rightarrow p^+\pi^0$

The SCS decays $\Lambda_c^+ \rightarrow p\eta$ and $p\pi^0$ have not yet been studied experimentally. These two decays proceed predominantly through internal W -emission and W -exchange diagrams, which are non-factorizable and not subject to color and helicity suppression in charmed baryon decay. Some theoretical models [34, 35, 36, 37], predict the BFs of these two process under different assumptions (the flavor SU(3) symmetry, FSI) obtaining different results. Therefore, measurements of these BFs will help us to understand the underlying dynamics of charmed baryon decays and distinguish between the different models. Furthermore, the ratio of BFs of these two decays, which is expected to be relatively insensitive to the values of input parameters in the theoretical calculation, is an excellent probe to distinguish between the different models.

We measure the BFs of $\Lambda_c^+ \rightarrow p\eta$ and $p\pi^0$ by using ST method, η is reconstructed by the two sub-mode $\eta \rightarrow \gamma\gamma$ and $\eta \rightarrow \pi^+\pi^-\pi^0$. The fitting plots can be found in Fig. 4. The corresponding BFs are calculated using $\mathcal{B}_{\Lambda_c^+ \rightarrow p\eta} = \frac{N_{\text{sig}}}{2 \cdot N_{\Lambda_c^+ \bar{\Lambda}_c^-} \cdot \epsilon \cdot \mathcal{B}_{\text{inter}}}$, where N_{sig} is the signal yield determined from the M_{BC} fit, $N_{\Lambda_c^+ \bar{\Lambda}_c^-} = (105.9 \pm 4.8(\text{stat.}) \pm 0.5(\text{syst.})) \times 10^3$ is the total number of $\Lambda_c^+ \bar{\Lambda}_c^-$ pairs in the data [32], ϵ is the detection efficiency estimated by the MC simulation, and $\mathcal{B}_{\text{inter}}$ is the η or π^0 decay BF taken from the PDG [10]. The factor of 2 in the denominator accounts for

the charge conjugation of the Λ_c^+ . The resultant BF of $\Lambda_c^+ \rightarrow p\eta$ is determined to be $\mathcal{B}_{\Lambda_c^+ \rightarrow p\eta} = (1.24 \pm 0.28(\text{stat.}) \pm 0.10(\text{syst.})) \times 10^{-3}$, uncertainties are statistical and systematic, respectively.

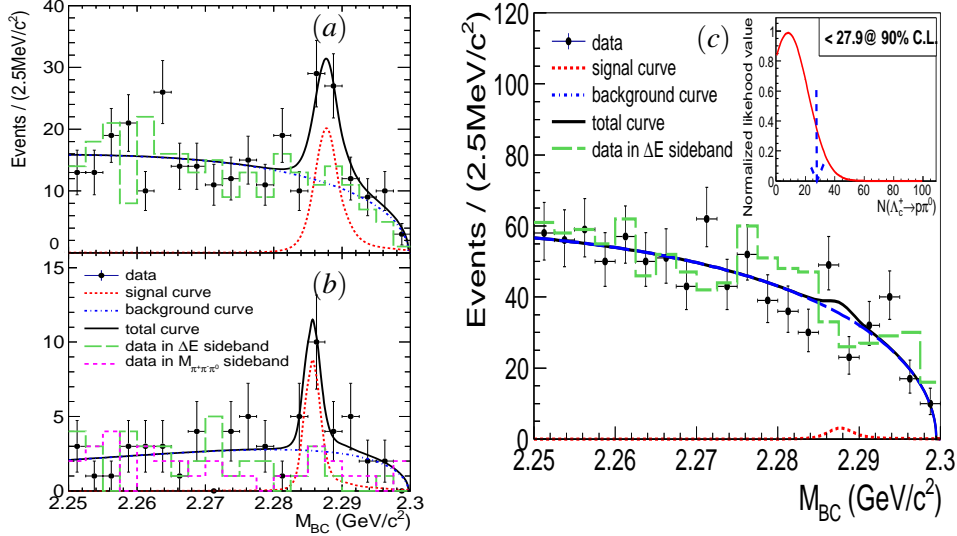


Figure 4: (color online) Simultaneous fit to the M_{BC} distributions of $\Lambda_c^+ \rightarrow p\eta$ reconstructed with the decay modes (a) $\eta \rightarrow \gamma\gamma$, (b) $\eta \rightarrow \pi^+\pi^-\pi^0$ and (c) $\Lambda_c^+ \rightarrow p\pi^0$. The dots with error bars are data, the (black) solid curves are for the best fits, the (blue) dash-dotted curves are for the backgrounds, and the (red) dashed curves are for the signals. The (green) long-dashed histograms and (pink) dashed histogram (in (b) only) are the data in the ΔE and $M_{\pi^+\pi^-\pi^0}$ sideband region. In (c), the insert shows the normalized likelihood distribution, which includes the systematic uncertainty, as a function of the expected signal yield. The (blue) dashed arrow indicates the upper limit on the signal yield at 90% C.L.

Since no significant $\Lambda_c^+ \rightarrow p\pi^0$ signal is observed, an upper limit on the BF is estimated. The upper limit at the 90% C.L. on the BF is calculated by substituting η with π^0 , which is 2.7×10^{-4} . The corresponding ratio of BFs between the two decays is also calculated to be $\mathcal{B}_{\Lambda_c^+ \rightarrow p\pi^0} / \mathcal{B}_{\Lambda_c^+ \rightarrow p\eta} < 0.24$, where the common uncertainties are cancelled. The measured BFs and their ratio are compared to the theoretical predictions from different models. More details can be found in Ref. [38].

3.4 Measurement of $\Lambda_c^+ \rightarrow \Lambda + X$ (preliminary)

The inclusive decay $\Lambda_c^+ \rightarrow \Lambda + X$, where X means any possible final state particles, is mediated by the $c \rightarrow s$ Cabibbo-favored transition that dominates the decays of Λ_c^+ . The measurement of BF of this decay, $\mathcal{B}_{\Lambda_c^+ \rightarrow \Lambda + X} = (35 \pm 11)\%$ [10] has a relatively low precision and has not been updated since 1992. It is crucial to improve the accuracy of the BF of the decay $\Lambda_c^+ \rightarrow \Lambda + X$, which allows us to understand the quark structure and decay dynamics of the least massive charmed baryon. In addition, it can also provide an essential input for exploring the decays of the b -flavored hadrons involving a Λ_c^+ in the final states. We also search for the direct CP violation by measuring the charge asymmetry of this inclusive decay $\mathcal{A}_{CP} = \frac{\mathcal{B}_{\Lambda_c^+ \rightarrow \Lambda_c X^-} - \mathcal{B}_{\Lambda_c^- \rightarrow \Lambda_c X}}{\mathcal{B}_{\Lambda_c^+ \rightarrow \Lambda_c X} + \mathcal{B}_{\Lambda_c^- \rightarrow \Lambda_c X}}$.

DT method is used in this analysis. Only $\Lambda_c^+ \rightarrow pK_S^0$ and $\Lambda_c^+ \rightarrow pK^- \pi^+$ are tagged to suppress the non- Λ_c background. Then we search for a Λ among the remaining tracks. We extract the signal

by fitting the M_{BC} distribution and subtract the sideband. The BF of $\Lambda_c^+ \rightarrow \Lambda_c X$ is determined to be $\mathcal{B}_{\Lambda_c^+ \rightarrow \Lambda_c X} = (38.2_{-2.2}^{+2.8} \pm 0.6)\%$, where the uncertainties are statistical and systematic, respectively. The precision of the BF is improved by a factor of 4, compared to the previous measurement. The CP asymmetry of the decay $\Lambda_c^+ \rightarrow \Lambda_c X$ is obtained by comparing the separate BFs of the charge conjugate decays, which are $\mathcal{B}_{\Lambda_c^+ \rightarrow \Lambda_c X} = (39.4_{-3.4}^{+4.7})\%$ and $\mathcal{B}_{\bar{\Lambda}_c^- \rightarrow \bar{\Lambda}_c X} = \pm(37.8_{-2.9}^{+3.8})\%$. The CP asymmetry is determined to be $\mathcal{A}_{CP} = (2.1_{-6.6}^{+7.0})\%$, where the uncertainty is statistical only. The direct CP violation in this decay is measured for the first time. The precision is limited by statistical uncertainty and no evidence for CP violation is found.

References

- [1] M. Ablikim et al. (BESIII Collaboration), Nucl. Instrum. Methods Phys. Res. A 614, 345 (2010).
- [2] R. M. Baltrusaitis et al. (MARK III Collaboration), Phys. Rev. Lett. 56, 2140 (1986).
- [3] I.I. Bigi and H. Yamamoto, Phys. Lett. B 349, 363 (1995).
- [4] Z. Z. Xing, Phys. Rev. D 55, 196 (1997).
- [5] Q. He et al. (CLEO Collaboration), Phys. Rev. Lett. 100, 091801 (2008).
- [6] M. Ablikim et al. (BESIII Collaboration), Phys. Lett. B 744, 339 (2015).
- [7] F. Buccella et al. (CLEO Collaboration), Phys. Lett. B. 302, 319 (1993); F. Buccella et al. Phys. Rev. D 51, 3478 (1995); M. Golden and B. Grinstein, Phys. Lett. B 222, 501 (1989).
- [8] S. Bianco et al. Riv. Nuovo. Cim. 26N7-8, 1 (2003); A. Le Yaouanc et al. Phys. Lett. B. 292, 353 (1992)
- [9] K. Arms et al. (CLEO Collaboration), Phys. Rev. D. 69, 071102 (2004).
- [10] K. A. Olive et al. (Particle Data Group) Chin. Phys. C 38, 090001 (2014).
- [11] G. Bonvicini et al. (CLEO Collaboration), Phys. Rev. D. 77, 091106(R) (2008).
- [12] L.-L. Chau and H.-Y. Cheng, Phys. Rev. D 36, 137 (1987); H.-Y. Cheng and C.-W. Chiang, *ibid.* 81, 074021 (2010).
- [13] K. Waikwok and S. Rosen, Phys. Lett. B 298, 413 (1993).
- [14] Y. Grossman and D. J. Robinson, J. High Energy Phys. 2013, 67 (2013).
- [15] F.-S. Yu, X.-X. Wang, and C.-D. Lařu, Phys. Rev. D 84, 074019 (2011).
- [16] H.-n. Li, C.-D. Lu, and F.-S. Yu, Phys. Rev. D 86,036012 (2012).
- [17] X. Y. Pham *et al.*, Phys. Lett. B 193, 331 (1987).
- [18] R. E. Karlsen and M. D. Scadron *et al.*, Phys. Rev. D 45, 4113 (1992).
- [19] Y. S. Dai *et al.*, Phys. Rev. D 60, 014014 (1999).
- [20] J. O. Eeg *et al.*, Phys. Rev. D 64, 034010 (2001).
- [21] W. Kwong and S. P. Rosen, Phys. Lett. B 298, 413 (1993).
- [22] H. N. Li *et al.*, Phys. Rev. D 86, 036012 (2012).
- [23] S. Müller *et al.*, Phys. Rev. D 92, 014004 (2015).

- [24] A. Biswas *et al.*, Phys. Rev. D 92, 014032 (2015).
- [25] M. Ablikim *et al.* (BESIII Collaboration), Chin. Phys. C 37, 123001 (2013); Phys. Lett. B **753**, 629 (2016).
- [26] G. Bonvicini *et al.* (CLEO Collaboration), Phys. Rev. D 89, 072002 (2014).
- [27] M. Ablikim *et al.* (BESIII Collaboration), Phys. Lett. B 765, 231 (2017).
- [28] G. S. Abrams *et al.* (Mark II Collaboration), Phys. Rev. Lett. 44 10 (1980).
- [29] M. Ablikim *et al.* (BESIII Collaboration), Phys. Lett. B 772, 288 (2017).
- [30] H. Y. Cheng, Front. Phys. 10, 101406 (2015).
- [31] H. Y. Cheng and C. W. Chiang, Phys. Rev. D 81, 074021 (2010).
- [32] M. Ablikim *et al.* (BESIII Collaboration), Phys. Rev. Lett. 116, 052001 (2016).
- [33] M. Ablikim *et al.* (BESIII Collaboration), Phys. Rev. Lett. 117, 232002 (2016)
- [34] K. K. Sharma, R. C. Verma, Phys. Rev. D 55, 7067 (1997).
- [35] T. Uppal, R. C. Verna, M. P. Khanna, Phys. Rev. D 49, 3417 (1994).
- [36] S. L. Chen, X. H. Guo, X. Q. Li and G. L. Wang, Commun. Theor. Phys. 40, 563 (2003)
- [37] Cai-Dian Lü, Wei Wang, and Fu-Sheng Yu, Phys. Rev. D 93, 056008 (2016).
- [38] M. Ablikim *et al.* (BESIII Collaboration), Phys. Rev D 95, 111102 (2017).
- [39] J. G. Körner, G. Kramer and J. Willrodt, Phys. Lett. B 279 78, 492 (1978) Erratum: [Phys. Lett. B 81, 419 (1979)]